JCB Journal of Cell Biology

ARTICLE

TORC2 controls endocytosis through plasma membrane tension

Margot Riggi[1,2,3,4], Clélia Bourgoint[1], Mariano Macchione[4,5], Stefan Matile[4,5], Robbie Loewith[1,3,4], and Aurélien Roux[2,4]

Target of rapamycin complex 2 (TORC2) is a conserved protein kinase that regulates multiple plasma membrane (PM)–related processes, including endocytosis. Direct, chemical inhibition of TORC2 arrests endocytosis but with kinetics that is relatively slow and therefore inconsistent with signaling being mediated solely through simple phosphorylation cascades. Here, we show that in addition to and independently from regulation of the phosphorylation of endocytic proteins, TORC2 also controls endocytosis by modulating PM tension. Elevated PM tension, upon TORC2 inhibition, impinges on endocytosis at two different levels by (1) severing the bonds between the PM adaptor proteins Sla2 and Ent1 and the actin cytoskeleton and (2) hindering recruitment of Rvs167, an N-BAR–containing protein important for vesicle fission to endocytosis sites. These results underline the importance of biophysical cues in the regulation of cellular and molecular processes.

Introduction

Endocytosis is the process by which eukaryotic cells internalize material and information from their environment and recycle plasma membrane (PM) lipids, trafficking proteins, and cell-surface receptors. Membrane remodeling by a well-established sequence of protein complexes (Fig. S1 A) is essential to form endocytic buds that will internalize material (Kaksonen and Roux, 2018). Thus, the PM can be considered as a core part of the endocytic machinery. It is now broadly accepted that physical forces, in particular PM tension, participate in the regulation of the balance between exocytosis and endocytosis in various systems (Dai and Sheetz, 1995; Gauthier et al., 2012). Functioning in a homeostatic feedback loop, the opposing effects of endocytosis and exocytosis on PM area is generally believed to enable cells to keep tension close to a set point (Morris and Homann, 2001; Apodaca, 2002; Fernandez-Sanchez et al., 2015). Additionally, PM tension was shown to regulate specific steps of the endocytosis process, including clathrin pit formation by varying the membrane budding energy (Boulant et al., 2011; Saleem et al., 2015) and membrane fission by dynamin (Morlot et al., 2012). These tensile forces, depending on the geometry of the bud, constitute either a basal constraint that the cell machinery has to counteract or a driving force in order to reshape the PM and form the endocytic vesicle.

Membrane remodeling during endocytosis requires energy. In most mammalian cells, coat proteins are sufficient to drive membrane invagination. However, in yeast cells, which have a high turgor pressure, the dynamic polymerization of actin is additionally required to power PM invagination (Kaksonen et al., 2006; Aghamohammadzadeh and Ayscough, 2009; Basu et al., 2014; Dmitrieff and Nédélec, 2015). In mammalian cells, such an extra force is only needed under conditions where the energy requirements of PM bending are increased, for example at the apical face of polarized epithelial cells (Gottlieb et al., 1993), where membrane bending rigidity is higher, or when membrane tension is increased, as in the case of osmotic swelling or mechanical stretching of cells (Boulant et al., 2011).

Target of rapamycin complex 2 (TORC2) was first implicated in the regulation of endocytosis almost 20 yr ago when screens for mutants defective in ligand-stimulated internalization of the α-factor receptor identified alleles of *TOR2* and *YPK1*, which encodes an AGC-family kinase and direct substrate of TORC2 (deHart et al., 2002, 2003). The characterization of TORC2 signaling outputs affecting endocytosis was facilitated only recently with the development of chemical-genetic approaches to specifically and acutely inhibit this complex (Gaubitz et al., 2015; Rispal et al., 2015; Bourgoint et al., 2018). This revealed that TORC2 regulates endocytosis both through rapid phosphorylation cascades largely mediated by the phospholipid flippase kinases Fpk1 and Fpk2 (Rispal et al., 2015; Roelants et al., 2017b; Bourgoint et al., 2018) and through a slower route presumably

[1]Department of Molecular Biology, University of Geneva, Geneva, Switzerland; [2]Department of Biochemistry, University of Geneva, Geneva, Switzerland; [3]iGE3 Institute of Genetics and Genomics of Geneva, Geneva, Switzerland; [4]Swiss National Centre for Competence in Research Program Chemical Biology, Geneva, Switzerland; [5]Department of Organic Chemistry, University of Geneva, Geneva, Switzerland.

Correspondence to Robbie Loewith: robbie.loewith@unige.ch; Aurélien Roux: aurelien.roux@unige.ch.

involving changes in the biophysical properties of the PM (Rispal et al., 2015).

Independently, we recently demonstrated that TORC2 is a key player in the maintenance of PM tension homeostasis (Berchtold et al., 2012; Riggi et al., 2018), prompting us to speculate that the slower route through which TORC2 regulates endocytosis involves its control of PM tension (Rispal et al., 2015). Here, we show that this is indeed the case, independently of previously described phosphorylation cascades. Inhibition of TORC2 leads to a gradual climb in PM tension, and once a critical threshold is passed, the bonds between the endocytic adaptor proteins and actin filaments fail and coat protein internalization ceases. These phenomena are suppressed if membrane tension is artificially reduced and mimicked if tension is elevated through orthogonal approaches. Lastly, we show that increased tension also blocks the recruitment of Rvs167 to endocytic sites, suggesting that the binding of this BAR-domain protein is highly sensitive to membrane curvature.

Results

TORC2 inhibition induces the appearance of actin comet tails and the clustering of endocytosis sites

Gradual depletion of TORC2 activity has long been known to lead to an eventual blockade of endocytosis in yeast (deHart et al., 2002, 2003). As endocytosis-related proteins are recruited to, and dissociate from, the budding site in a precise and well-orchestrated order (Kaksonen et al., 2005), we can use them as an internal temporal ladder to study endocytosis dynamics. Here, we followed, as kymographs and time-lapse series (Fig. 1 A), the residency times of the actin-binding protein Abp1 at the PM, together with either the coat protein Sla1 or the fission-regulating protein Rvs167. When we analyzed single endocytic events, we found that in mock-treated cells, consistent with previous results (Kaksonen et al., 2005; Kukulski et al., 2012), all proteins localized to punctate cortical foci. Sla1 resided at an endocytic patch for ∼30–40 s, and Abp1 was recruited for a total of ∼20 s, with an ∼10-s overlap with Sla1. Rvs167 was in turn recruited for ∼10 s and disassembled shortly before Abp1, as the patch budded into the cytoplasm, representing completion of a successful endocytic event (Fig. 1, B and C; and Videos 1 and 2). We used cells expressing *TOR1-1* S1972R missense mutation that prevents FKBP12-Rapamycin binding to Tor1, thus conferring TORC1 resistance to Rapamycin, in combination with deletion leading to the removal of the C-terminal part of Avo3, a subunit unique to TORC2, to generate a strain expressing a Rapamycin-sensitive TORC2 variant, as described previously (Gaubitz et al., 2015). Acute chemical-genetic inhibition of TORC2 extended all residency times of the proteins at the PM to the point that endocytic patches often failed to resolve during the time of the experiment (Fig. 1, D and E; and Videos 3 and 4). Strikingly, we also observed the appearance of Abp1 "comet tails" instead of normal punctate cortical patches. These were anchored to an endocytosis site at the cell cortex (marked by an immobile Sla1 patch) and continuously waved back and forth in the cytoplasm. These structures are typical of an uncoupling between the PM and the actin cytoskeleton (Kaksonen et al., 2003; Skruzny et al., 2012). Moreover, we observed that most of the blocked endocytic sites were clustered at one given location of the cell, whereas endocytosis events are usually evenly distributed along the PM of a (nonbudding) cell (Fig. 1, D and E). Finally, TORC2 inhibition also seemed to affect the recruitment of Rvs167 to the PM, as the corresponding patches were much dimmer and did not always colocalize with Abp1 (Fig. 1 E and Video 4).

When studying in more detail the kinetics of the endocytosis failure upon TORC2 inhibition (Fig. S1, B and C), we observed a significant increase in the lifetime of the protein patches only after 30 min (Fig. 1, F–H). The same amount of time was necessary to observe a significant amount of cells displaying clustered endocytosis sites and a "comet tail" phenotype (Fig. 1 I). Notably, the decrease in intensity of Rvs167 foci was already observable after 15 min, suggesting that it is not a consequence of the blockade of earlier endocytosis steps. These relatively slow kinetics are difficult to explain based solely by changes in protein phosphorylation (Rispal et al., 2015; Roelants et al., 2017b; Bourgoint et al., 2018).

The actin comet tail phenotype associated with TORC2 inhibition is due to increased PM tension

We hypothesized that the slow and progressive appearance of clustered actin comet tails is the consequence of the increase of PM tension that follows TORC2 inhibition (Riggi et al., 2018). This parameter can now be easily evaluated by fluorescent lifetime imaging microscopy (FLIM) through the lifetime of the Flipper-TR probe (Colom et al., 2018), and we observed that both phenomena (appearance of actin comet tails and rise in PM tension) follow similar kinetics (Figs. 2 A and S2 A).

To test this assumption, we investigated whether increased PM tension induced through orthologous means could trigger a similar phenotype. We recently demonstrated that osmotic shocks can be used to manipulate PM tension in yeast (Riggi et al., 2018). As WT yeast cells adapt within a few minutes to a hypo-osmotic shock, we used *FPS1Δ* cells that cannot efficiently export the osmo-protectant glycerol (Beese et al., 2009); indeed, upon hypo-osmotic shocks, their PM tension does not increase significantly more than in WT cells, but it is slower to recover (Fig. S2, B and C).

As hypothesized, a hypo-osmotic shock induced the formation of actin comet tails anchored to a blocked endocytic site marked by a nonmotile Sla1 patch (Fig. 2 B and Video 5), and the clustering of endocytosis sites (Figs. 2 C and S2 D). A hypo-osmotic shock also mimicked the defects in Rvs167 recruitment at the PM (Fig. 2 D and Video 6), and the foci that still formed after the shock were on average half as bright (Fig. 2 E). Importantly, a hypo-osmotic shock had a more transient but similar effect on Rvs167 in WT cells (Fig. S2 E), arguing against a peculiar behavior of *ΔFPS1* mutants. These phenomena were similar to those observed upon TORC2 inhibition but differed in one important regard: they were manifest within seconds (in contrast to the 15–30 min required following TORC2 inhibition), which is coherent with the fast increase of PM tension upon this treatment (Fig. S2 C).

Conversely, we examined whether the uncoupling phenotype caused by TORC2 inhibition could be rescued by

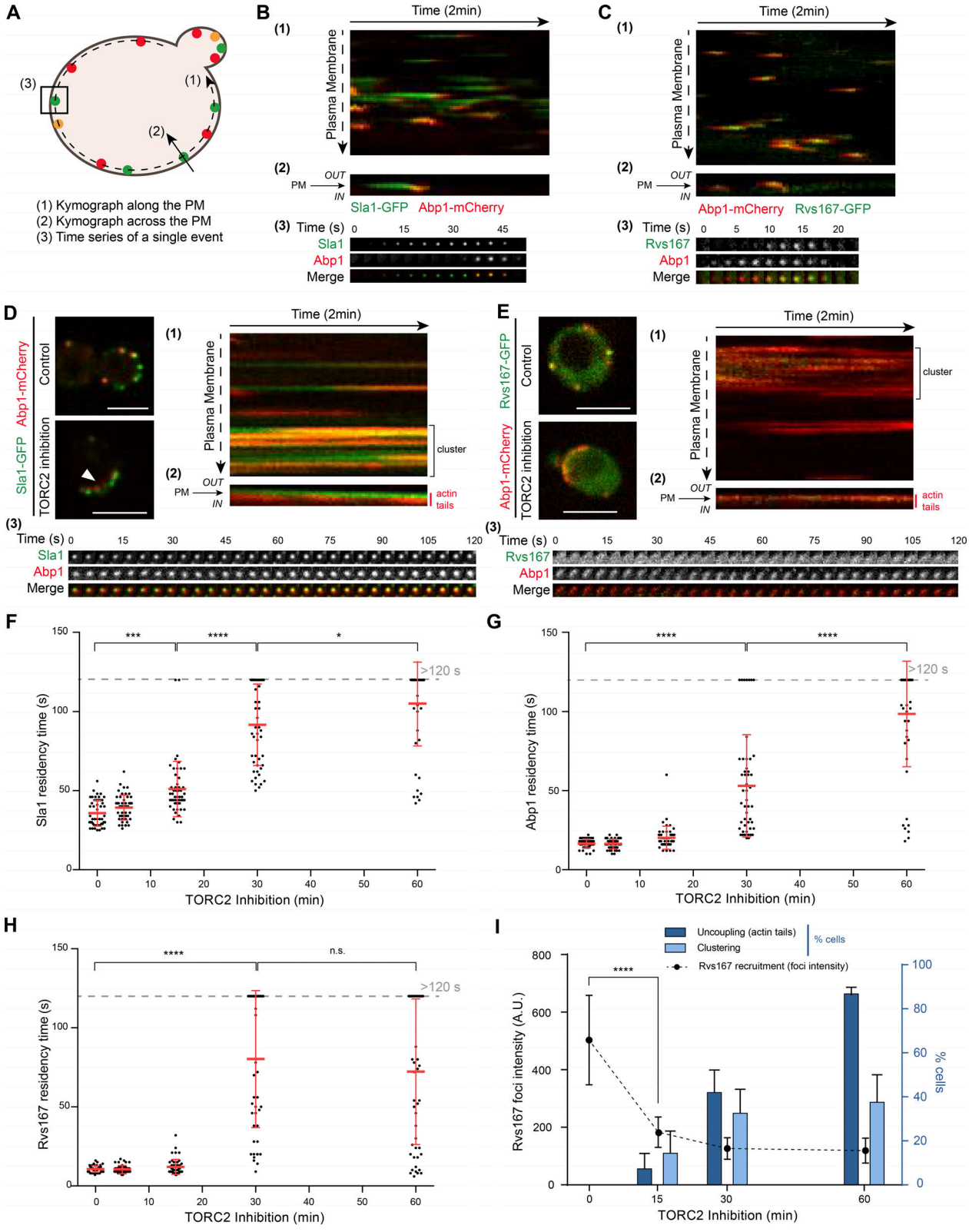

Figure 1. **TORC2 inhibition affects endocytosis at multiple stages. (A)** Illustration explaining how the kymographs and time series were obtained. **(B–E)** Kymographs recorded either along (1) or across (2) the PM and time series of a single endocytic event (3) showing Abp1-mCherry signal and either Sla1-GFP (B and D) or Rvs167-GFP (C and E). They were recorded before (B and C) and after (D and E) TORC2 inhibition by 1-h Rapamycin treatment in *TOR1-1 AVO3Δ^{CT}* cells. The arrowhead is pointing at actin tails (D). **(F–H)** Evolution of the PM residency times of Sla1 (F), Abp1 (G), and Rvs167 (H), upon TORC2 inhibition in *TOR1-1 AVO3Δ^{CT}* cells. Error bars represent SD of mean values calculated for $n = 50$ events from at least three independent experiments (****, $P < 0.0001$; ***, $P < 0.001$; *, $P < 0.05$). n.s., not significant. **(I)** Evolution of Rvs167-GFP foci intensity and the percentage of cells displaying either an uncoupling phenotype or clustered endocytosis sites upon TORC2 inhibition in *TOR1-1 AVO3Δ^{CT}* cells. Error bars represent SD of mean values calculated from three independent experiments (with $n > 100$ cells or $n > 150$ foci; ****, $P < 0.0001$). Scale bars, 5 µm. Source data are provided in Table S1.

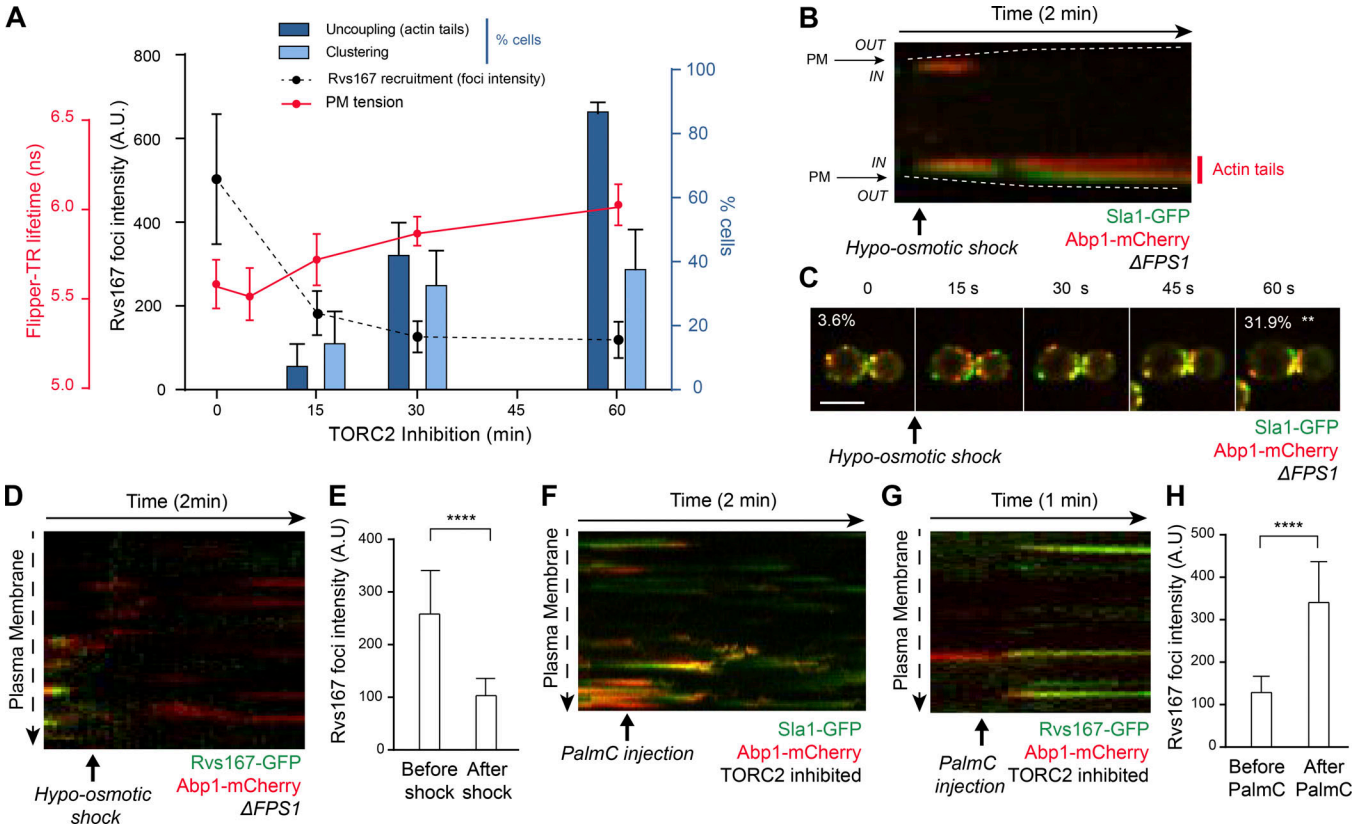

Figure 2. **The uncoupling phenotype and Rvs167 misrecruitment are due to an increase in PM tension. (A)** Correlation between the kinetics of the increase in PM tension upon TORC2 inhibition and appearance of the various endocytosis phenotypes. PM tension was monitored through the lifetime of the FliptR probe measured by FLIM, and error bars represent the propagated error of mean values calculated from three independent experiments (with $n > 10$ cells). **(B)** Sla1-GFP and Abp1-mCherry kymograph recorded across a *FPS1Δ* cell upon hypo-osmotic shock. Dot lines represent the PM. **(C)** Time series of merged Sla1-GFP and Abp1-mCherry signals in *FPS1Δ* cells upon hypo-osmotic shock. The percentage of cells presenting clustered endocytosis sites are indicated before and after the shock and were calculated from three independent experiments (**, $P < 0.01$). **(D)** Rvs167-GFP and Abp1-mCherry kymograph along the PM of a *FPS1Δ* cell upon hypo-osmotic shock. **(E)** Average intensity of Rvs167-GFP foci before and after hypo-osmotic shock. Error bars represent SD of mean values calculated for $n = 100$ events from three independent experiments (****, $P < 0.0001$). **(F and H)** Abp1-mCherry and either Sla1-GFP (F) or Rvs167-GFP (H) kymographs recorded as indicated along the PM of a *TOR1-1 AVO3Δ^{CT}* cell, pretreated with Rapamycin for 1 h, upon PalmC injection. **(G)** Average intensity of Rvs167-GFP foci before and after PalmC treatment in a *TOR1-1 AVO3Δ^{CT}* cell, pretreated with Rapamycin for 1 h. Error bars represent SD of mean values calculated for $n = 100$ events from three independent experiments (****, $P < 0.0001$). Scale bars, 5 µm. Source data are provided in Table S1.

artificially decreasing PM tension through Palmitoylcarnitine (PalmC) treatment (Riggi et al., 2018). Although the lifetime of the endocytic patches at the PM remained on average longer than in control cells, likely because TORC2 also regulates endocytosis through other pathways (i.e., phosphorylation cascades) that are still affected, PalmC addition induced the disassembly of the actin comet tails and the redistribution of clustered endocytic patches (Fig. 2 F and Video 7). This suggests that these latter two features are controlled by TORC2 via PM tension, whereas the elongation of the patch lifetime is likely also influenced by the down-regulation of related phosphorylation cascades. In accordance with a previous study, which could rescue endocytosis defects with hyperosmotic shocks in various mutants, but not in *SLA2Δ* cells (Basu et al., 2014), PalmC treatment did not rescue the uncoupling phenotype due to *SLA2* deletion (Fig. S2 F). As *SLA2Δ* cells do not exhibit a particularly high PM tension under basal conditions and still exhibit a decrease of PM tension upon PalmC treatment (Fig. S2 G), we hypothesize that, in this case, the phenotype is rather due to complete loss of the physical link between the PM and the cytoskeleton. Consistently, Ent1 has been shown to require Sla2 to stably bind to the PM (Skruzny et al., 2012, 2015).

Decreasing PM tension through PalmC treatment could also partially rescue the defects in Rvs167 recruitment (Fig. 2 G and Video 8); even if the residency time of the patches was still longer than in basal conditions, they became, within a few seconds, more than twice brighter (Fig. 2 H).

Together, these observations demonstrate that PM tension increase (caused by TORC2 inhibition) is sufficient to trigger PM/cytoskeleton uncoupling. Moreover, they confirm the importance of the level of PM tension for an efficient recruitment of Rvs167.

TORC2 connects to endocytosis through two parallel pathways

TORC2 signaling is also connected to endocytosis via the flippase kinases Fpk1 and Fpk2 and downstream phosphorylation

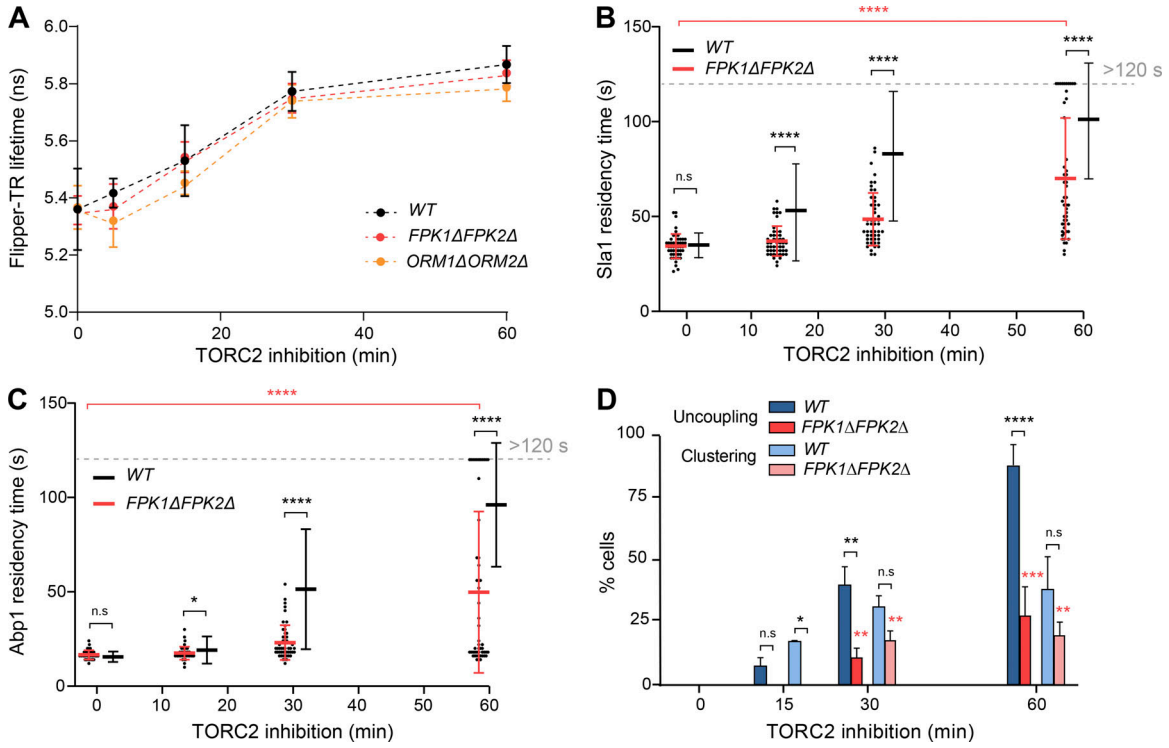

Figure 3. **TORC2 connects to endocytosis through two parallel pathways. (A)** Evolution of PM tension, monitored through the lifetime of the Flipper-TR probe measured by FLIM, upon TORC2 inhibition by Rapamycin treatment in *TOR1-1 AVO3Δ^{CT}*, *TOR1-1 AVO3Δ^{CT} FPK1Δ FPK2Δ*, or *TOR1-1 AVO3Δ^{CT} ORM1Δ ORM2Δ* cells. Error bars represent the propagated error of mean values calculated from three independent experiments (with $n > 10$ cells). **(B and C)** Evolution of the PM residency times of Sla1 (B) or Abp1 (C) upon TORC2 inhibition in *TOR1-1 AVO3Δ^{CT} FPK1Δ FPK2Δ* cells. Error bars represent SD of mean values calculated for $n = 50$ events from at least three independent experiments (*, $P < 0.05$; ****, $P < 0.0001$; indicated in black when calculated to the WT at the same time point and in red when calculated to the initial time point of the *FPK1Δ FPK2Δ* cells). **(D)** Evolution of the percentage of cells displaying either an uncoupling phenotype or clustered endocytosis sites upon TORC2 inhibition in *TOR1-1 AVO3Δ^{CT} FPK1Δ FPK2Δ* cells. Error bars represent SD of mean values calculated from three independent experiments (with $n > 50$ cells; *, $P < 0.05$; **, $P < 0.01$; ***, $P < 0.001$; ****, $P < 0.0001$; indicated in black when calculated to the WT at the same time point and in red when calculated to the initial time point of the *FPK1Δ FPK2Δ* cells). Scale bars, 5 µm. n.s., not significant. Source data are provided in Table S1.

cascades (Rispal et al., 2015; Roelants et al., 2017b; Bourgoint et al., 2018). Phosphorylation cascades downstream of TORC2 are affected relatively quickly by Rapamycin treatment, which maximally inhibits TORC2 after 5 min (Fig. S3 A), and are thus unlikely to be solely responsible for the uncoupling phenotype. To test the possibility that previously described effects of TORC2 on endocytic protein phosphorylation could still influence the present phenotype, we used the *ΔFPK1ΔFPK2* mutant, which is known to rescue the phosphorylation-dependent effects of TORC2 inhibition on endocytosis (Rispal et al., 2015). Importantly, TORC2 inhibition induced a similar increase in PM tension in this mutant (Fig. 3 A), meaning that Fpk-related effects are not sufficient to account for the control of PM tension by TORC2. In accordance to previous observations (Rispal et al., 2015), the double deletion of *FPK1* and *FPK2* partially rescued endocytosis defects at intermediate time points but to a much lesser extent at later time points (Fig. 3, B–D). The fact that this rescue is not complete argues for the existence of an additional pathway, independent of these kinases, connecting TORC2 to endocytosis (i.e., through the regulation of PM tension).

Consistently, increasing PM tension through hypo-osmotic shock did not cause any detectable change in Pan1 phosphorylation (Fig. S3 B). Thus, the uncoupling phenotype due to increased PM tension is not the consequence of an alteration of the phosphorylation of the adaptor proteins, which are hypo-phosphorylated upon TORC2 inhibition (Roelants et al., 2017b; Bourgoint et al., 2018).

One major output of TORC2 signaling is the regulation of sphingolipid biosynthesis (Eltschinger and Loewith, 2016; Roelants et al., 2017a), in part through the phosphorylation of regulatory proteins Orm1 and Orm2 by Ypk1 (Roelants et al., 2011). Previously, we had hypothesized that TORC2 regulates tension via this pathway (Rispal et al., 2015). However, PM tension increases upon TORC2 inhibition in a *ΔORM1ΔORM2* mutant similarly to WT (Fig. 3 A), suggesting that modulation of sphingolipid biosynthesis is not sufficient to explain TORC2-mediated control of PM tension. In addition, we could not observe any spatial heterogeneity in FLIM images of Flipper-TR staining after either TORC2 inhibition (Fig. S2 A) or hypo-osmotic shock (Fig. S2 B) that could connect potential large-scale changes in lipid organization at the PM to the observed clustering phenotype.

Collectively, these observations demonstrate that two parallel pathways can be delineated, control of PM tension and Fpk-dependent phosphorylation events, through both of which TORC2 coordinately regulates endocytosis.

The adaptor proteins Sla2 and Ent1/2 are present at blocked endocytic sites upon TORC2 inhibition

Actin comet tails were previously observed in *SLA2Δ* (Kaksonen et al., 2003) or *ENT1ΔENT2Δ* (Carroll et al., 2012) deletion mutants. These adaptor proteins were shown to cooperatively link the PM to the actin cytoskeleton, efficiently transmitting the force generated by polymerizing actin to the PM. More precisely, Sla2 helps tether Ent1 to the endocytic coat, and, in the absence of Sla2, polymerizing actin pulls Ent1 off the PM (Skruzny et al., 2012). Consistently, the PM remains flat in cells where the Sla2-Ent1/2 link is disrupted (Picco et al., 2018).

We wondered whether TORC2 inhibition would also affect the behavior of the adaptor proteins Ent1 and Sla2. In untreated cells, the timing of Ent1 recruitment to the PM compared with Sla1 seemed quite variable (Fig. 4 A), which is consistent with the proposed greater flexibility of the early stages of endocytosis; in contrast, Ent1 patches assembled on average 25 s before Abp1 recruitment (Fig. 4 B). Upon TORC2 inhibition, Ent1 was still present at the PM and localized to blocked endocytic patches, here again often clustered to one position of the cell. It did not travel along the actin comet tails marked with Abp1 but rather remained at the PM with the nonmotile Sla1 patches (Fig. 4, A and B). Sla2 was similarly progressively blocked at the PM upon TORC2 inhibition and also did not travel along the actin comet tails (Fig. 4 C).

These observations suggest that the PM/cytoskeleton uncoupling phenotype observed upon TORC2 inhibition is due to defects in the link between the adaptor proteins and the actin cytoskeleton and not between the adaptor proteins and the PM.

Actin tails are the consequence of an imbalance between PM tension and the strength of its link to the cytoskeleton

We hypothesized that if PM tension becomes too high, then the bonds between the PM and actin filaments might be unable to support the force necessary to invaginate the membrane. To test this idea, we wondered whether weakening the link that couples the PM and the cytoskeleton would result in a faster appearance of the actin tails upon TORC2 inhibition. Single deletions of *ENT1* or *ENT2*, which encode epsin homologues, do not cause any obvious phenotype (Wendland et al., 1999); however, we postulated that it might nevertheless compromise the connection between the PM and the cytoskeleton. When we followed the evolution of PM tension upon TORC2 inhibition in *ENT1Δ* cells, we could not detect any significant difference compared with WT cells (Fig. 5 A). However, the appearance of the extension of the PM residency time of Sla1 (Fig. 5 B) and Abp1 (Fig. 5 C), as well as the appearance of the uncoupling and the clustering phenotypes, were all faster (Fig. 5 D). This means that in the *ENT1Δ* mutant, a PM tension increase of lesser magnitude is sufficient to break the fewer and/or weaker remaining bonds between the PM and the cytoskeleton.

An alternative hypothesis might be that increased PM tension directly or indirectly impacts F-actin organization, but manipulations of F-actin with drugs stabilizing or destabilizing filaments could not mimic (Fig. S4, A and B) or rescue (Fig. S4, C and D) the effects of TORC2 inhibition on endocytosis. To confirm that the assembly of actin filaments was not the root cause of the endocytic defect, we engineered a strain in which the interactions between the adaptor proteins and the PM were compromised, our thinking being that in this strain, background, the adaptor proteins should now travel with actin waves upon TORC2 inhibition. To this end, we replaced endogenous *ENT1* with a plasmid-borne ent1 allele expressing an N-terminally truncated protein lacking the PM-binding domain. As predicted, the truncated Ent1$^{\Delta N}$ flared along with actin tails upon TORC2 inhibition (Fig. 5 E), whereas under similar conditions, the full-length protein remained associated with the PM as a punctate structure (Fig. 4, A and B). This observation confirms that actin filaments are still able to bind Ent1 upon TORC2 inhibition, and therefore, that the uncoupling phenotype is not due to defects in actin filaments organization or function.

Together, these results demonstrate that PM tension is a crucial parameter governing endocytosis in yeast. Indeed, the connecting bridge transmitting the force developed by the cytoskeleton to actively reshape the PM and pull it inward can only support a finite amount of force, above which it breaks and actin polymerization becomes futile.

Discussion

Previous work had already postulated that TORC2 regulates endocytosis both through direct phosphorylation cascades largely mediated by the phospholipid flippase kinases Fpk1 and 2 and through changes in the biophysical properties of the PM (Rispal et al., 2015; Roelants et al., 2017b; Bourgoint et al., 2018). Here, we confirmed that some of the endocytic defects observed in TORC2-inhibited cells, specifically the recruitment of Rvs167 and the uncoupling between the PM and the cytoskeleton, are due to an increase in PM tension, independent of Fpk-related phosphorylation events. More precisely, the latter phenomenon is the consequence of the breakage of the connecting bonds between the adaptor proteins and actin filaments upon increased tension (Fig. 5 F). This underlines the importance of biophysical cues in the regulation of cellular and molecular processes. Although we had previously suggested that TORC2 regulated membrane tension via sphingolipid biosynthesis (Rispal et al., 2015), deletion of the *ORM1/2* genes did not prevent PM tension increase upon TORC2 inhibition. TORC2 is now appreciated to regulate many targets that could impinge upon membrane tension (Eltschinger and Loewith, 2016; Roelants et al., 2017a), and it is likely through the collection of these downstream effectors that TORC2 inhibition results in increased membrane tension.

We observed that the PM tension has to increase, and be maintained for an amount of time, before the actin cytoskeleton uncouples from the PM. This threshold can be seen as the maximum force that the links among the PM, adaptor proteins and cytoskeleton can withstand. This threshold can be artificially decreased by weakening this connection (e.g., through *ENT1* single deletion). Conversely, this threshold needs to be held for a longer period of time in the absence of Fpk1/2-mediated phosphorylation events, demonstrating that TORC2 regulates endocytosis synergistically through convergent pathways (i.e., signaling cascades and tension).

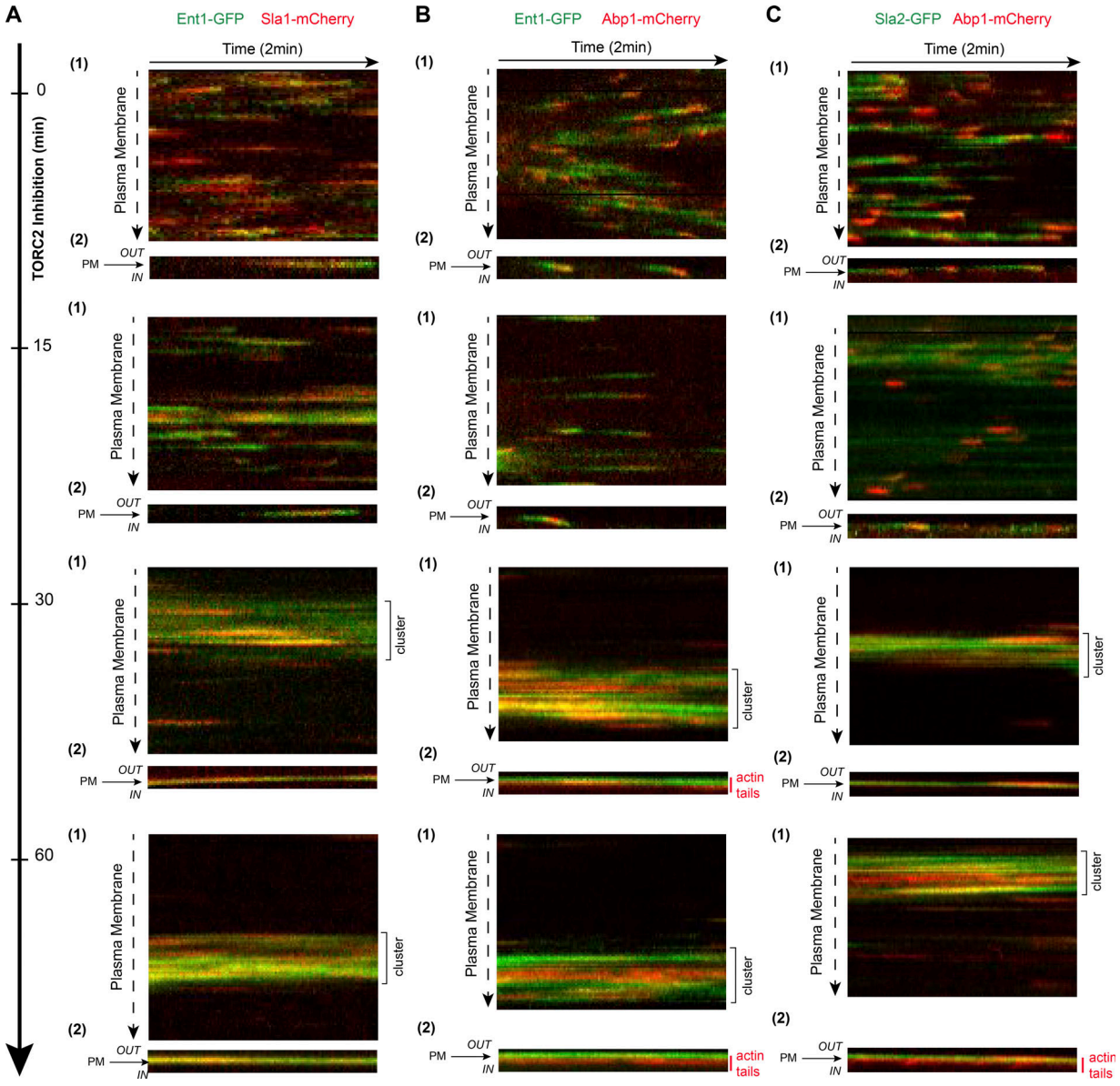

Figure 4. **Ent1 colocalizes with blocked endocytosis sites, but not actin tails, upon TORC2 inhibition. (A–C)** Kymographs of the indicated tagged proteins after the indicated time of TORC2 inhibition by Rapamycin treatment in *TOR1-1 AVO3Δ^{CT}*. Kymographs were recorded either along (1) or across (2) the PM. Scale bars, 5 µm.

The adaptors Sla2 and Ent1/2 constitute a physical bridge between the PM and the actin cytoskeleton; each of these proteins possesses a PtdIns(4,5)P_2-binding domain in its N-terminal part and, in the case of Sla2, a THATCH/talin-like domain in its C-terminal end (Skruzny et al., 2012). The Ent1–actin interaction domain is additionally known to be regulated by phosphorylation by kinases of the Ark family (Skruzny et al., 2012), which are also potential downstream targets of TORC2 (Rispal et al., 2015; Bourgoint et al., 2018). However, as the uncoupling phenotype is largely rescued by an artificial decrease of PM tension induced by PalmC, a condition in which TORC2 inhibition is maintained, it is more probably the direct mechanical effect of increased PM tension rather than, or in addition to, a consequence of the TORC2-related down-regulated phosphorylation cascades that causes this phenotype.

Our results support the notion that actin polymerization provides force, transmitted through the adaptor proteins, to pull the membrane into the cell interior against PM tension due to turgor pressure. The weak link in this force-transducing chain appears to be the connection between the adaptor proteins and the actin cytoskeleton, but this can be changed if mutations that weaken the PM–adaptor interactions are introduced (Ent1$^{\Delta N}$). This observation demonstrates that actin polymerization per se is functional in the absence of TORC2 activity/high membrane tension but endocytosis fails due to rupture of protein–protein interactions.

Notably, the defect in Rvs167 recruitment to endocytic foci appears faster than all the other phenotypes, whereas the kinetics of the increase of its residency time is similar to other proteins. This suggests that TORC2 might impinge on this

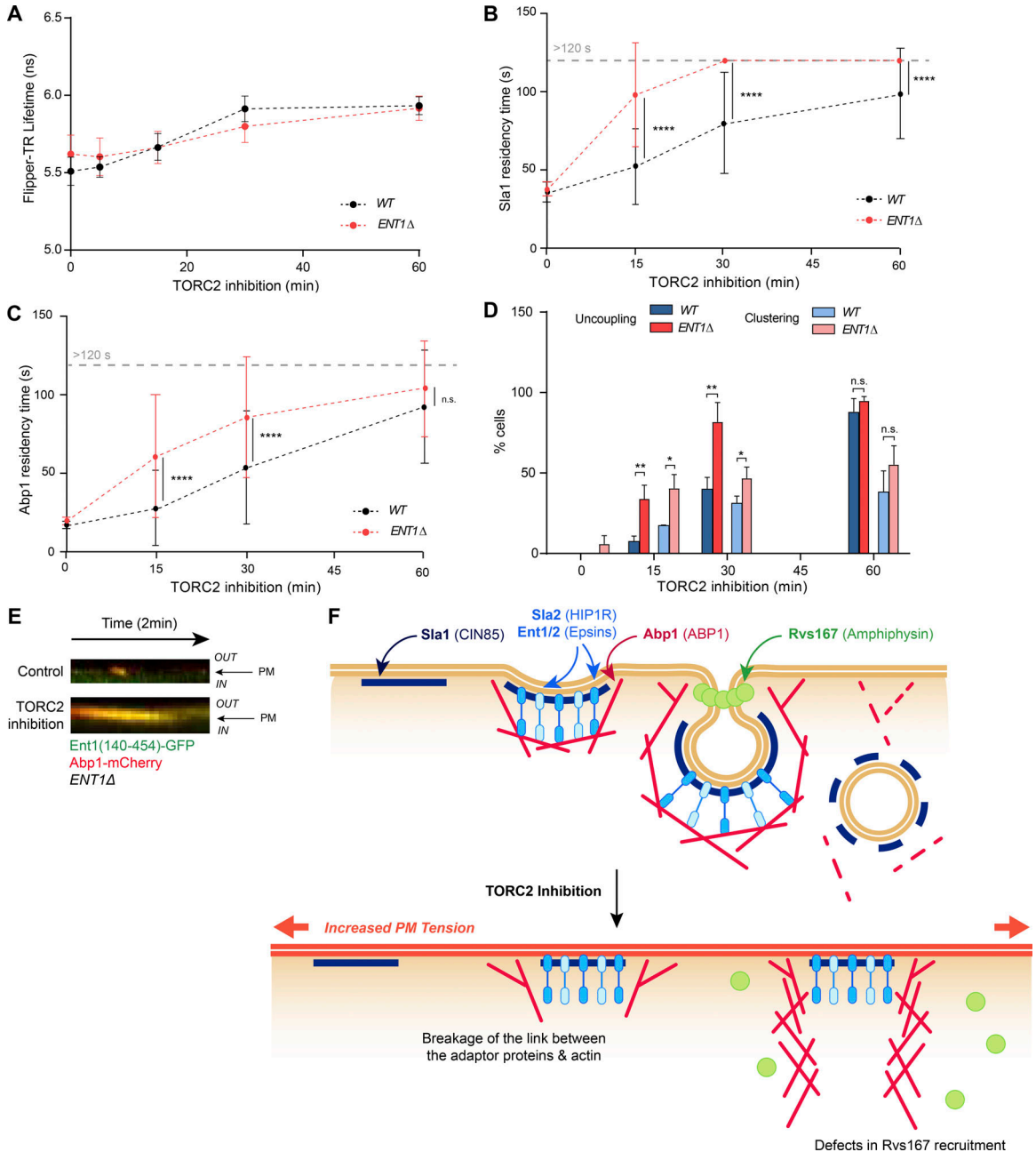

Figure 5. **The uncoupling phenotype is the consequence of an unbalance between PM tension and the force that the adaptor proteins can sustain.** **(A)** Evolution of PM tension, monitored through the lifetime of the Flipper-TR probe measured by FLIM, upon TORC2 inhibition in *TOR1-1 AVO3Δ^{CT}* cells deleted or not of *ENT1*. Error bars represent the propagated error of mean values calculated from three independent experiments (with $n > 10$ cells). **(B and C)** Comparison of the evolution of the PM residency times of Sla1 (B) or Abp1 (C) upon TORC2 inhibition in *TOR1-1 AVO3Δ^{CT}* cells deleted or not of *ENT1*. Error bars represent SD of mean values calculated for $n = 100$ events from at least three independent experiments (****, $P < 0.0001$). **(D)** Comparison of the kinetics of appearance of the uncoupling phenotype upon TORC2 inhibition in *TOR1-1 AVO3Δ^{CT}* cells deleted or not of *ENT1*. Error bars represent SD of mean values calculated for $n = 100$ events from at least three independent experiments (*, $P < 0.05$; **, $P < 0.01$). n.s., not significant. **(E)** Deleting PM-binding N-terminal domain of Ent1 results in its colocalization with actin tails. Kymographs recorded across the PM showing Ent1(140–454)-GFP and Abp1-mCherry signals before and after 30 min of TORC2 inhibition. **(F)** Model illustrating that TORC2 inhibition induces an increase in PM tension that affects endocytosis at several levels.

process through an additional pathway in parallel to the increase in PM tension. Indeed, Rvs167 binding to the PM is known to be sensitive not only to PM biophysical properties such as curvature (Youn et al., 2010; Simunovic et al., 2015) but also to its composition, specifically to the level of complex sphingolipids (Youn et al., 2010), which is also regulated by TORC2 (Aronova et al., 2008; Breslow et al., 2010; Roelants et al., 2011; Muir et al., 2014).

Another striking phenotype associated with TORC2 inhibition is the clustering of the endocytic sites. This could also be recapitulated by increasing PM tension through orthologous means and conversely rescued by decreasing PM tension,

Table 1. **Strains used in this study**

Strain	Genotype	Reference
TB50	MATα *leu2-3,112 ura3-52 rme1 trp1 his3*	Wullschleger et al., 2005
Mpr8	TB50α *TOR1-1* avo3Δ1274-1430::HphMX6	Gaubitz et al., 2015
MR14	TB50α *TOR1-1* avo3Δ1274-1430::URA Sla1-GFP::HIS3 Abp1-mCherry::KanMx6	This study
MR116	TB50α *TOR1-1* avo3Δ1274-1430::URA Rvs167-GFP::HIS3 Abp1-mCherry::KanMx6	This study
MR21	TB50α *TOR1-1* avo3Δ1274-1430::URA Ent1-GFP::HIS3 Abp1-mCherry::KanMx6	This study
MR20	TB50α *TOR1-1* avo3Δ1274-1430::URA Ent1-GFP::HIS3 Sla1-mCherry::KanMx6	This study
MR79	TB50α *TOR1-1* avo3Δ1274-1430::URA Sla2-GFP::HIS3 Abp1-mCherry::KanMx6	This study
MR117	TB50α *TOR1-1* avo3Δ1274-1430::URA Sla1-GFP::HIS3 Abp1-mCherry::KanMx ent1Δ::TRP1	This study
MKY1195	MATa, his3Δ200, leu2-3,112, ura3-52, lys2-801, sla2:natNT2, SLA1-EGFP::HIS3MX6, ABP1-mCherry::kanMX4	Skruzny et al., 2012
MR124	TB50α, *TOR1-1* avo3Δ1274-1430::URA ORM1::HIS ORM2::TRP1	This study
MR123	TB50α, *TOR1-1* avo3Δ1274-1430::URA Fpk1::TRP1 Fpk2::TRP1 Abp1-mCherry::Kan Sla1-GFP::HIS	This study
MR125	TB50α *TOR1-1* avo3Δ1274-1430::URA Abp1-mCherry::KanMx6 ent1Δ::TRP1	This study

suggesting that here again, increased PM tension is the direct cause of the clustering. We can hypothesize that the assembly of a first endocytosis patch facilitates the assembly of subsequent patches in the vicinity by locally modifying the biophysical properties of the PM.

The force developed by actin polymerization and its efficient transmission to the PM are of particular importance to power endocytosis in yeast, as the cells have to counteract a high turgor pressure, possibly due to their cell wall. Importantly, HeLa cells in which Sla2 mammalian homologue Hip1R is down-regulated display the same actin comet tail phenotype (Engqvist-Goldstein et al., 2004), as well as the cellular slime mold *Dictostelium discoideum* lacking epsins (Brady et al., 2010), meaning that the molecular mechanism of PM–actin cytoskeleton coupling is likely conserved across evolution. It would be interesting to investigate whether this connection is also under the influence of the PM tension in higher organisms and potentially of TORC2, as it has also been linked to PM tension regulation in higher eukaryotes (Diz-Muñoz et al., 2016).

Materials and methods

Yeast strains and plasmids

All strains used in this study are listed in Table 1. Yeast strains were generated either by homologous recombination of PCR-generated fragments as previously described or by crossing, sporulation, and subsequent dissection of the spores. All plasmids and primers used for the generation of the strains are listed in Tables 2 and 3. Strains were confirmed by PCR and sequencing. Cloning and site-directed mutagenesis were performed following standard procedures, and plasmids were verified by sequencing. All tagged proteins are functional and expressed from their endogenous promoter.

Yeast culture

Yeast cells were grown according to standard procedures at 30°C in Synthetic Complete medium to an early logarithmic phase. For the hypo-osmotic shocks, cells were grown in Synthetic Complete medium containing 1 M sorbitol, and prewarmed Synthetic Complete medium was injected inside a flow chamber.

Chemicals

Rapamycin (LC Laboratories) was dissolved in DMSO at 1 mg/ml and used at a final concentration of 200 nM. PalmC was dissolved in DMSO at 10 mM and used at 5 µM. The Flipper-TR probe, synthetized following reported procedures (Colom et al., 2018), was dissolved in DMSO and used at a final concentration of 2n g/ml. Latrunculin A (L5163; Sigma-Aldrich) and Phalloidin (A1488; Applichem) were dissolved in ethanol at 2 mM and 1 mg/ml respectively, and used at 1 µM.

Antibodies

The following antibodies were used in this study: rabbit anti-Ypk1 1:25,000 (homemade), mouse anti-phospho-Ypk1-T^{662} 1:500 (Berchtold et al., 2012), mouse anti-HA 1:15,000 (H9658; Sigma-Aldrich), polyclonal rabbit anti-phosphothreonine 1:1,000 (CN 71–8200; Thermo Fisher Scientific), and the appropriate infrared dye-coupled secondary antibodies used at a dilution of 1:10,000 (donkey IRDye680-conjugated anti-mouse 926–68072 and IRDye800-conjugated anti-rabbit 926–32213 secondary antibodies; LI-COR Biosciences).

Table 2. **Plasmids used in this study**

Plasmid	Description	Reference
p525	pFA6a-mCherry-kan	Lab stock
p16	pFA6a-GFP(S65T)-HIS3	Longtine et al., 1989
p12	pFA6a-TRP1	Longtine et al., 1989
pMS007	pRS416-Ent1(140-454)-2xHA-meGFP	Marko Kaksonen Lab; Skruzny et al., 2012
pMS082	pRS415-PAN1-5HA-TADH1	Bourgoint et al., 2018

Table 3. **Primers used in this study**

Name	Purpose	Sequence (5′–3′)
Sla1_F2	Cter tagging	CAACATATTCAATGCTACTGCATCAAATCCGTTTGGATTCCGGATCCCCGGGTTAATTAA
Sla1_R1	Cter tagging	GTTTTAGTTATTATCCTATAAAATCTTAAAATACATTAATGAATTCGAGCTCGTTTAAAC
Abp1_F2	Cter tagging	AAAAGGTCTCTTCCCCAGCAATTATGTGTCTTTGGGCAACCGGATCCCCGGGTTAATTAA
Abp1_R1	Cter tagging	ACGTAAGAATAATATAATAGCATGACGCTGACGTGTGATTGAATTCGAGCTCGTTTAAAC
Ent1_F2	Cter tagging	TAATGGCTCAAATAACCGGGGATATACTCTAATTGATTTACGGATCCCCGGGTTAATTAA
Ent1_R1	Deletion/Cter tagging	GCTCATCTGATTAGAAATGCGGACTGGAATGACAGAATCACTGAATTCGAGCTCGTTTAAAC
Ent1_F1	deletion	GCCAGGATCAGAAGGAAAGGGAGCAAGAGGCAGAACAATCCGGATCCCCGGGTTAATTAA
Sla2_F2	Cter tagging	AGAGATTGGGCGAGATAAGAAGGCATGCCTACTATAACCAGGATGATGATCGGATCCCCGGGTTAATTAA
Sla_R1	Cter tagging	ATATATTTATATTAACGTTTATCTTTATATATAAAAAGTACAATTCATGAGAATTCGAGCTCGTTTAAAC
Rvs167_F2	Cter tagging	AGGTGTGTTTCCTGGGAACTACGTGCAACTCAACAAGAACCGGATCCCCGGGTAAATTAA
Rvs167_R1	Cter tagging	AATAGAAGGTAATGAATACAGAGGGATGCAGGGGCCTCCTGAATTCGAGCTCGTTTAAAC

TCA protein extraction and phosphoproteins immunodetection

6% TCA was directly added to exponentially growing yeast cultures, and cells were incubated for 5 min on ice before collection. Protein extracts and immunoprecipitations were performed as previously described (Rispal et al., 2015). Briefly, 6% TCA was added to exponentially growing yeast cultures, and cells were incubated for 5 min on ice before collection. Cell lysis was performed in 100 µl of urea buffer (25 mM Tris, pH 6.8, 6 M urea, and 1% SDS) with glass beads (Retsch; Thermo Fisher Scientific) in a FastPrep bead beater (Lucerna-Chem). For immunoprecipitation experiments, extracts were diluted in IP buffer (PBS, 10%[vol/vol] glycerol, 0.5% Tween 20 supplemented with the complete protease inhibitor mixture containing EDTA [Roche Applied Science], and 1 mM PMSF), and the soluble fraction was incubated with mouse monoclonal anti-HA (H9658; Sigma-Aldrich)–coupled protein G Dynabeads (Invitrogen) for 3 h at 4°C. After incubation, the beads were washed twice with IP buffer, and bound proteins were released with addition of 1× SDS sample buffer containing 5% β-mercaptoethanol and incubation for 5 min at 95°C. Proteins were resolved on a 7.5% SDS gel and blotted on a nitrocellulose membrane. Immunodetection was performed using the indicated antibodies and the Odyssey IR imaging system (LI-COR Biosciences).

Confocal microscopy

Cells were grown at 30°C in Synthetic Complete (SC) medium to an early logarithmic phase, mounted on coverslips coated with 0.1 µg/ml Concanavalin A (Sigma-Aldrich), and immediately imaged with a spinning-disc microscope assembled by 3i (Intelligent Imaging Innovation) and Nikon (Eclipse C1; Nikon) using a 100× objective (NA = 1.3; Nikon). For microfluidics experiments, a Concanavalin A–coated coverslip was bonded to the bottom surface of a flow chamber (sticky-slide VI 0.4; Ibidi) with one entry connected to a syringe pump (Aladdin; World Precision Instruments) and the other left open for sequential introduction of different solutions. The flow chamber was primed with SC medium before the loading of cells. Loaded cells were washed several times with SC medium and then subjected to the appropriate treatments.

FLIM

Cells were grown overnight in Synthetic Complete medium to OD_{600} = 0.05 to 0.1, concentrated by spinning, and incubated for 1 min with 2 ng/ml of the Flipper-TR probe. FLIM imaging was performed using a Nikon Eclipse Ti A1R microscope equipped with a time-correlated single-photon counting module from PicoQuant58. Excitation was performed using a pulsed 485-nm laser (LDH-D-C-485; PicoQuant) operating at 20 MHz, and the emission signal was collected through a 600/50-nm bandpass filter using a gated PMA hybrid 40 detector and a TimeHarp 260 PICO board (PicoQuant).

Image processing and quantification

The acquired image series were background subtracted and corrected for general photobleaching. Final image processing and analysis were done using ImageJ.

The quantification of the uncoupling and clustering phenotypes was done manually.

For FLIM analysis (Figs. 2 A, 3 A, and 5 A; and Fig. S2, C and F), we used SymPhoTime 64 software (PicoQuant) to fit the data according to a two-exponential reconvolution model and calculate the lifetime of the Flipper-TR probe.

Statistics and reproducibility

The sample sizes and statistical tests were selected based on previous studies with similar methodologies. All experiments were repeated at least three times, giving similar results. The results of independent experiments are presented as mean values; error bars represent the SD or the propagated error when the value of each experiment was itself calculated as a mean of individual cells. Statistical significance was tested using the two-tailed *t* test.

Data availability

Source data for Fig. 1, E–I; Fig. 2, A, C, E, and H; Fig. 3, A–D; Fig. 5, A–D; Fig. S2, C and F; and Fig. S3 are provided in Table S1.

Online supplemental material

Fig. S1 shows that the effects of TORC2 inhibition on endocytosis are progressive. Fig. S2 shows that osmotic shocks and PalmC treatment affect PM tension in yeast. Fig. S3 shows that Fpk-related phosphorylation of endocytic proteins is independent of PM tension. Fig. S4 shows that F-actin manipulations through drug-stabilizing or destabilizing filaments do not mimic or rescue the uncoupling phenotype. Table S1 lists statistics source data. Video 1 shows *TOR1-1 AVO3Δ^{CT}* cells expressing Abp1-mCherry and Sla1-GFP. Video 2 shows *TOR1-1 AVO3Δ^{CT}* cells expressing Abp1-mCherry and Rvs167-GFP. Video 3 shows *TOR1-1 AVO3Δ^{CT}* cells expressing Abp1-mCherry and Sla1-GFP after 1-h TORC2 inhibition by Rapamycin treatment. Video 4 shows *TOR1-1 AVO3Δ^{CT}* cells expressing Abp1-mCherry and Rvs1671-GFP after 1-h TORC2 inhibition by Rapamycin treatment. Video 5 shows *TOR1-1 AVO3Δ^{CT}* cells expressing Abp1-mCherry and Sla1-GFP in 1 M sorbitol and submitted to a hypo-osmotic shock when indicated. Video 6 shows *TOR1-1 AVO3Δ^{CT}* cells expressing Abp1-mCherry and Rvs167-GFP in 1 M sorbitol and submitted to a hypo-osmotic shock when indicated. Video 7 shows *TOR1-1 AVO3Δ^{CT}* cells expressing Abp1-mCherry and Sla1-GFP after 1-h Rapamycin treatment and treated with 10 µM PalmC when indicated. Video 8 shows *TOR1-1 AVO3Δ^{CT}* cells expressing Abp1-mCherry and Rvs167-GFP after 1-h Rapamycin treatment and treatment with 10 µM PalmC when indicated.

Acknowledgments

The authors thank Marko Kaksonen and Andrea Picco for their advice and comments on the manuscript.

S. Matile, R. Loewith, and A. Roux acknowledge generous financial support from the Canton of Geneva, the Swiss National Science Foundation, and the National Centre of Competence in Research in Chemical Biology.

The FliptR probe is now commercially available under the name Flipper-TR from Spirochrome through the National Centre of Competence in Research Store (https://nccr-chembio.ch/technologies/nccr-store/).

The authors declare no competing financial interests.

Author contributions: M. Riggi wrote the first draft of the manuscript and performed most of the experiments, except the immunoprecipitations, which were performed by C. Bourgoint. M. Macchione synthesized the Flipper-TR probe under the direction and support of S. Matile. M. Riggi, R. Loewith, and A. Roux designed the experiments and edited the manuscript.

Submitted: 17 January 2019
Revised: 11 April 2019
Accepted: 6 May 2019

References

Aghamohammadzadeh, S., and K.R. Ayscough. 2009. Differential requirements for actin during yeast and mammalian endocytosis. *Nat. Cell Biol.* 11:1039–1042. https://doi.org/10.1038/ncb1918

Apodaca, G. 2002. Modulation of membrane traffic by mechanical stimuli. *Am. J. Physiol. Renal Physiol.* 282:F179–F190. https://doi.org/10.1152/ajprenal.2002.282.2.F179

Aronova, S., K. Wedaman, P.A. Aronov, K. Fontes, K. Ramos, B.D. Hammock, and T. Powers. 2008. Regulation of ceramide biosynthesis by TOR complex 2. *Cell Metab.* 7:148–158. https://doi.org/10.1016/j.cmet.2007.11.015

Basu, R., E.L. Munteanu, and F. Chang. 2014. Role of turgor pressure in endocytosis in fission yeast. *Mol. Biol. Cell.* 25:679–687. https://doi.org/10.1091/mbc.e13-10-0618

Beese, S.E., T. Negishi, and D.E. Levin. 2009. Identification of positive regulators of the yeast fps1 glycerol channel. *PLoS Genet.* 5:e1000738. https://doi.org/10.1371/journal.pgen.1000738

Berchtold, D., M. Piccolis, N. Chiaruttini, I. Riezman, H. Riezman, A. Roux, T.C. Walther, and R. Loewith. 2012. Plasma membrane stress induces relocalization of Slm proteins and activation of TORC2 to promote sphingolipid synthesis. *Nat. Cell Biol.* 14:542–547. https://doi.org/10.1038/ncb2480

Boulant, S., C. Kural, J.C. Zeeh, F. Ubelmann, and T. Kirchhausen. 2011. Actin dynamics counteract membrane tension during clathrin-mediated endocytosis. *Nat. Cell Biol.* 13:1124–1131. https://doi.org/10.1038/ncb2307

Bourgoint, C., D. Rispal, M. Berti, I. Filipuzzi, S.B. Helliwell, M. Prouteau, and R. Loewith. 2018. Target of rapamycin complex 2-dependent phosphorylation of the coat protein Pan1 by Akl1 controls endocytosis dynamics in *Saccharomyces cerevisiae*. *J. Biol. Chem.* 293:12043–12053. https://doi.org/10.1074/jbc.RA117.001615

Brady, R.J., C.K. Damer, J.E. Heuser, and T.J. O'Halloran. 2010. Regulation of Hip1r by epsin controls the temporal and spatial coupling of actin filaments to clathrin-coated pits. *J. Cell Sci.* 123:3652–3661. https://doi.org/10.1242/jcs.066852

Breslow, D.K., S.R. Collins, B. Bodenmiller, R. Aebersold, K. Simons, A. Shevchenko, C.S. Ejsing, and J.S. Weissman. 2010. Orm family proteins mediate sphingolipid homeostasis. *Nature.* 463:1048–1053. https://doi.org/10.1038/nature08787

Carroll, S.Y., H.E. Stimpson, J. Weinberg, C.P. Toret, Y. Sun, and D.G. Drubin. 2012. Analysis of yeast endocytic site formation and maturation through a regulatory transition point. *Mol. Biol. Cell.* 23:657–668. https://doi.org/10.1091/mbc.e11-02-0108

Colom, A., E. Derivery, S. Soleimanpour, C. Tomba, M.D. Molin, N. Sakai, M. González-Gaitán, S. Matile, and A. Roux. 2018. A fluorescent membrane tension probe. *Nat. Chem.* 10:1118–1125. https://doi.org/10.1038/s41557-018-0127-3

Dai, J., and M.P. Sheetz. 1995. Mechanical properties of neuronal growth cone membranes studied by tether formation with laser optical tweezers. *Biophys. J.* 68:988–996. https://doi.org/10.1016/S0006-3495(95)80274-2

deHart, A.K., J.D. Schnell, D.A. Allen, and L. Hicke. 2002. The conserved Pkh-Ypk kinase cascade is required for endocytosis in yeast. *J. Cell Biol.* 156:241–248. https://doi.org/10.1083/jcb.200107135

deHart, A.K., J.D. Schnell, D.A. Allen, J.Y. Tsai, and L. Hicke. 2003. Receptor internalization in yeast requires the Tor2-Rho1 signaling pathway. *Mol. Biol. Cell.* 14:4676–4684. https://doi.org/10.1091/mbc.e03-05-0323

Diz-Muñoz, A., K. Thurley, S. Chintamen, S.J. Altschuler, L.F. Wu, D.A. Fletcher, and O.D. Weiner. 2016. Membrane Tension Acts Through PLD2 and mTORC2 to Limit Actin Network Assembly During Neutrophil Migration. *PLoS Biol.* 14:e1002474. https://doi.org/10.1371/journal.pbio.1002474

Dmitrieff, S., and F. Nédélec. 2015. Membrane Mechanics of Endocytosis in Cells with Turgor. *PLOS Comput. Biol.* 11:e1004538. https://doi.org/10.1371/journal.pcbi.1004538

Eltschinger, S., and R. Loewith. 2016. TOR Complexes and the Maintenance of Cellular Homeostasis. *Trends Cell Biol.* 26:148–159. https://doi.org/10.1016/j.tcb.2015.10.003

Engqvist-Goldstein, A.E., C.X. Zhang, S. Carreno, C. Barroso, J.E. Heuser, and D.G. Drubin. 2004. RNAi-mediated Hip1R silencing results in stable association between the endocytic machinery and the actin assembly machinery. *Mol. Biol. Cell.* 15:1666–1679. https://doi.org/10.1091/mbc.e03-09-0639

Fernandez-Sanchez, M.E., T. Brunet, J.C. Röper, and E. Farge. 2015. Mechanotransduction's impact on animal development, evolution, and tumorigenesis. *Annu. Rev. Cell Dev. Biol.* 31:373–397. https://doi.org/10.1146/annurev-cellbio-102314-112441

Gaubitz, C., T.M. Oliveira, M. Prouteau, A. Leitner, M. Karuppasamy, G. Konstantinidou, D. Rispal, S. Eltschinger, G.C. Robinson, S. Thore, et al. 2015. Molecular Basis of the Rapamycin Insensitivity of Target Of Rapamycin Complex 2. *Mol. Cell.* 58:977–988. https://doi.org/10.1016/j.molcel.2015.04.031

Gauthier, N.C., T.A. Masters, and M.P. Sheetz. 2012. Mechanical feedback between membrane tension and dynamics. *Trends Cell Biol.* 22:527–535. https://doi.org/10.1016/j.tcb.2012.07.005

Gottlieb, T.A., I.E. Ivanov, M. Adesnik, and D.D. Sabatini. 1993. Actin microfilaments play a critical role in endocytosis at the apical but not the basolateral surface of polarized epithelial cells. *J. Cell Biol.* 120:695–710. https://doi.org/10.1083/jcb.120.3.695

Kaksonen, M., and A. Roux. 2018. Mechanisms of clathrin-mediated endocytosis. *Nat. Rev. Mol. Cell Biol.* 19:313–326. https://doi.org/10.1038/nrm.2017.132

Kaksonen, M., Y. Sun, and D.G. Drubin. 2003. A pathway for association of receptors, adaptors, and actin during endocytic internalization. *Cell.* 115: 475–487. https://doi.org/10.1016/S0092-8674(03)00883-3

Kaksonen, M., C.P. Toret, and D.G. Drubin. 2005. A modular design for the clathrin- and actin-mediated endocytosis machinery. *Cell.* 123:305–320. https://doi.org/10.1016/j.cell.2005.09.024

Kaksonen, M., C.P. Toret, and D.G. Drubin. 2006. Harnessing actin dynamics for clathrin-mediated endocytosis. *Nat. Rev. Mol. Cell Biol.* 7:404–414. https://doi.org/10.1038/nrm1940

Kukulski, W., M. Schorb, M. Kaksonen, and J.A. Briggs. 2012. Plasma membrane reshaping during endocytosis is revealed by time-resolved electron tomography. *Cell.* 150:508–520. https://doi.org/10.1016/j.cell.2012.05.046

Longtine, M.S., N.M. Wilson, M.E. Petracek, and J. Berman. 1989. A yeast telomere binding activity binds to two related telomere sequence motifs and is indistinguishable from RAP1. *Curr. Genet.* 16:225–239. https://doi.org/10.1007/BF00422108

Morlot, S., V. Galli, M. Klein, N. Chiaruttini, J. Manzi, F. Humbert, L. Dinis, M. Lenz, G. Cappello, and A. Roux. 2012. Membrane shape at the edge of the dynamin helix sets location and duration of the fission reaction. *Cell.* 151:619–629. https://doi.org/10.1016/j.cell.2012.09.017

Morris, C.E., and U. Homann. 2001. Cell surface area regulation and membrane tension. *J. Membr. Biol.* 179:79–102. https://doi.org/10.1007/s002320010040

Muir, A., S. Ramachandran, F.M. Roelants, G. Timmons, and J. Thorner. 2014. TORC2-dependent protein kinase Ypk1 phosphorylates ceramide synthase to stimulate synthesis of complex sphingolipids. *eLife.* 3:e03779. https://doi.org/10.7554/eLife.03779

Picco, A., W. Kukulski, H.E. Manenschijn, T. Specht, J.A.G. Briggs, and M. Kaksonen. 2018. The contributions of the actin machinery to endocytic membrane bending and vesicle formation. *Mol. Biol. Cell.* 29:1346–1358. https://doi.org/10.1091/mbc.E17-11-0688

Riggi, M., K. Niewola-Staszkowska, N. Chiaruttini, A. Colom, B. Kusmider, V. Mercier, S. Soleimanpour, M. Stahl, S. Matile, A. Roux, and R. Loewith. 2018. Decrease in plasma membrane tension triggers PtdIns(4,5)P_2 phase separation to inactivate TORC2. *Nat. Cell Biol.* 20:1043–1051. https://doi.org/10.1038/s41556-018-0150-z

Rispal, D., S. Eltschinger, M. Stahl, S. Vaga, B. Bodenmiller, Y. Abraham, I. Filipuzzi, N.R. Movva, R. Aebersold, S.B. Helliwell, and R. Loewith. 2015. Target of Rapamycin Complex 2 Regulates Actin Polarization and Endocytosis via Multiple Pathways. *J. Biol. Chem.* 290:14963–14978. https://doi.org/10.1074/jbc.M114.627794

Roelants, F.M., D.K. Breslow, A. Muir, J.S. Weissman, and J. Thorner. 2011. Protein kinase Ypk1 phosphorylates regulatory proteins Orm1 and Orm2 to control sphingolipid homeostasis in Saccharomyces cerevisiae. *Proc. Natl. Acad. Sci. USA.* 108:19222–19227. https://doi.org/10.1073/pnas.1116948108

Roelants, F.M., K.L. Leskoske, M.N. Martinez Marshall, M.N. Locke, and J. Thorner. 2017a. The TORC2-Dependent Signaling Network in the Yeast Saccharomyces cerevisiae. *Biomolecules.* 7:E66. https://doi.org/10.3390/biom7030066

Roelants, F.M., K.L. Leskoske, R.T.A. Pedersen, A. Muir, J.M. Liu, G.C. Finnigan, and J. Thorner. 2017b. TOR Complex 2-Regulated Protein Kinase Fpk1 Stimulates Endocytosis via Inhibition of Ark1/Prk1-Related Protein Kinase Akl1 in Saccharomyces cerevisiae. *Mol. Cell. Biol.* 37: e00627-16. https://doi.org/10.1128/MCB.00627-16

Saleem, M., S. Morlot, A. Hohendahl, J. Manzi, M. Lenz, and A. Roux. 2015. A balance between membrane elasticity and polymerization energy sets the shape of spherical clathrin coats. *Nat. Commun.* 6:6249. https://doi.org/10.1038/ncomms7249

Simunovic, M., G.A. Voth, A. Callan-Jones, and P. Bassereau. 2015. When Physics Takes Over: BAR Proteins and Membrane Curvature. *Trends Cell Biol.* 25:780–792. https://doi.org/10.1016/j.tcb.2015.09.005

Skruzny, M., T. Brach, R. Ciuffa, S. Rybina, M. Wachsmuth, and M. Kaksonen. 2012. Molecular basis for coupling the plasma membrane to the actin cytoskeleton during clathrin-mediated endocytosis. *Proc. Natl. Acad. Sci. USA.* 109:E2533–E2542. https://doi.org/10.1073/pnas.1207011109

Skruzny, M., A. Desfosses, S. Prinz, S.O. Dodonova, A. Gieras, C. Uetrecht, A.J. Jakobi, M. Abella, W.J. Hagen, J. Schulz, et al. 2015. An organized co-assembly of clathrin adaptors is essential for endocytosis. *Dev. Cell.* 33: 150–162. https://doi.org/10.1016/j.devcel.2015.02.023

Wendland, B., K.E. Steece, and S.D. Emr. 1999. Yeast epsins contain an essential N-terminal ENTH domain, bind clathrin and are required for endocytosis. *EMBO J.* 18:4383–4393. https://doi.org/10.1093/emboj/18.16.4383

Wullschleger, S., R. Loewith, W. Oppliger, and M.N. Hall. 2005. Molecular organization of target of rapamycin complex 2. *J. Biol. Chem.* 280: 30697–30704. https://doi.org/10.1074/jbc.M505553200

Youn, J.Y., H. Friesen, T. Kishimoto, W.M. Henne, C.F. Kurat, W. Ye, D.F. Ceccarelli, F. Sicheri, S.D. Kohlwein, H.T. McMahon, and B.J. Andrews. 2010. Dissecting BAR domain function in the yeast Amphiphysins Rvs161 and Rvs167 during endocytosis. *Mol. Biol. Cell.* 21:3054–3069. https://doi.org/10.1091/mbc.e10-03-0181